A Comparison of Standard Coherence Models for Inflow Turbulence With Estimates from Field Measurements

Korn Saranyasoontorn

Lance Manuel

Department of Civil Engineering,
University of Texas at Austin,
Austin, Texas 78712 USA

Paul S. Veers

Wind Energy Technology Department,
Sandia National Laboratories,
Albuquerque, New Mexico 87185 USA

The Long-term Inflow and Structural Test (LIST) program, managed by Sandia National Laboratories, Albuquerque, NM, is gathering inflow and structural response data on a modified version of the Micon 65/13 wind turbine at a site near Bushland, Texas. With the objective of establishing correlations between structural response and inflow, previous studies have employed regression and other dependency analyses to attempt to relate loads to various inflow parameters. With these inflow parameters that may be thought of as single-point-in-space statistics that ignore the spatial nature of the inflow, no significant correlation was identified between load levels and any single inflow parameter or even any set of such parameters, beyond the mean and standard deviation of the hub-height horizontal wind speed. Accordingly, here, we examine spatial statistics in the measured inflow of the LIST turbine by estimating the coherence for the three turbulence components (along-wind, across-wind, and vertical). We examine coherence spectra for both lateral and vertical separations and use the available ten-minute time series of the three components at several locations. The data obtained from spatial arrays on three main towers located upwind from the test turbine as well as on two additional towers on either side of the main towers consist of 291 ten-minute records. Details regarding estimation of the coherence functions from limited data are discussed. Comparisons with standard coherence models available in the literature and provided in the International Electrotechnical Commission (IEC) guidelines are also discussed. It is found that the Davenport exponential coherence model may not be appropriate especially for modeling the coherence of the vertical turbulence component since it fails to account for reductions in coherence at low frequencies and over large separations. Results also show that the Mann uniform shear turbulence model predicts coherence spectra for all turbulence components and for different lateral separations better than the isotropic von Kármán model. Finally, on studying the cross-coherence among pairs of turbulence components based on field data, it is found that the coherence observed between along-wind and vertical turbulence components is not predicted by the isotropic von Kármán model while the Mann model appears to overestimate this cross-coherence. [DOI: 10.1115/1.1797978]

Keywords: Coherence, Inflow, Turbulence.

I Introduction

The present study was motivated by failure to find meaningful correlation between turbine loads (extremes and fatigue) and simple inflow parameters that did not describe the spatial structure of the inflow. For example, in previous regression studies by Nelson et al. [1] it was found that single-point-in-space statistics of inflow (e.g., at the hub height) were insufficient for predicting wind turbine loads such as extreme edgewise (in-plane) or flapwise (out-of-plane) bending moments at the blade root. It was, thus, thought to be useful to study the full spatial description of the random inflow turbulence field. The availability of inflow data (as time series segments) at multiple locations through the Long-term Inflow and Structural Test (LIST) program offers a unique opportunity to estimate the spatial statistics of the inflow. It is our belief that future studies on the correlation of wind turbine loads to inflow may be improved if such spatial statistics are taken into consideration.

One means of identifying the frequency-dependent and random nature of interactions in the inflow at different locations and how these might influence turbine loads is to study the coherence of along-wind (u), across-wind (v), and vertical (w) turbulence components. For design purposes, prescribed models for each turbulence component, including power spectra and coherence spectra, are required in order to perform simulations of the complete inflow field. Computational aerodynamic analysis software uses this simulated inflow to compute the structural response that may be used to determine design loads. Different theoretical turbulence models utilized to construct full-field wind simulation may result in significant differences in design loads for wind turbines. Veldkamp [2] compared predictions of turbine tower and blade fatigue loads based on inflow simulation with several turbulence models. For example, with two of the models studied—the Mann uniform shear model [3] where the spectral tensor for atmospheric surface layer turbulence in neutral conditions based on the Navier-Stokes equations as well as conservation of mass is modeled; and the Veers model [4] where the three turbulence components, contrary to the Mann model, are assumed independent—he concluded that predicted fatigue design loads were quite different. This finding suggests the importance of selecting appropriate turbulence models in design. We are also therefore interested in assessing the validity of the existing turbulence spectral models currently defined in the International Electrotechnical Commission (IEC) standard [5] as well as of other well-established coherence models

Contributed by the Solar Energy Division of the THE AMERICAN SOCIETY OF MECHANICAL ENGINEERS for publication in the ASME JOURNAL OF SOLAR ENERGY ENGINEERING. Manuscript received by the ASME Solar Energy Division, Jan. 2004; final revision, June, 2004. Editor: P. Chaviaropoulos.

available in the literature by comparing them with coherence spectra of full-field wind turbulence components estimated directly from field measurements from the LIST program managed by Sandia National Laboratories, Albuquerque, NM.

Another motivation for the present study is that although several field studies of the coherence structure of turbulence have been carried out in Europe (see, for example, Mann et al. [6]; Schlez and Infield [7]; Larsen and Hansen [8]), comparatively far fewer such studies, especially with the appropriate heights and separation distances that are useful for wind turbine applications, and that take into account site-dependent turbulence length scales have been carried out in the United States where the environmental conditions and coherence structure of the inflow may be different.

Recent findings from inflow measurements carried out in Europe by Larsen and Hansen [8] reveal that coherence of the along-wind turbulence component for different vertical separations decreases with increasing separation, with decreasing integral length scales, and with decreasing measuring altitudes. In contrast, for lateral separations, the same dependence of coherence on altitude was observed as was seen for vertical separations; however, no clear dependence of coherence on integral length scale and on spatial separation was identified based on the measurements. However, these conclusions are based upon limited data and the lateral separation distances in that study were greater than 79 m (much larger than the separations that we will study). Also, in that study, only the along-wind coherence was considered. Here, the available inflow data from the LIST program allow us to analyze coherence spectra for all three turbulence components at different vertical and lateral separations. In addition, we also study the cross-coherence of each pair of distinct turbulence components at the center of the rotor circle.

In the following, power spectra and coherence spectra for the three turbulence components are estimated using several of the LIST data sets by employing the Welch's modified Periodogram (block-averaging) spectral estimation method. To facilitate understanding of the coherence as a function of primary inflow parameters, we study these separately for different bins defined on the basis of hub-height mean and standard deviation values of horizontal wind speed. Since only limited data from the first phase of the LIST program were used and the estimations of the coherence functions may be subject to large statistical uncertainty, error statistics of the estimated spectra defined in terms of bias, variance, and confidence limits are discussed.

II LIST Data Set

The data sets employed to estimate spatial coherence spectra throughout this study were provided by Sandia National Laboratories through the ongoing Long-Term Inflow and Structural Test (LIST) program (Sutherland et al. [9], Jones et al. [10]). The LIST program has made available continuous time series of atmospheric inflow conditions as well as structural response data for a modified Micon 65/13 wind turbine (referred to as the LIST turbine in this study). This measurement campaign is taking place at the United States Department of Agriculture-Agricultural Research Service (USDA-ARS) site in Bushland, Texas which is characteristic of a Great Plains site with essentially flat terrain and the primary wind direction at the site is from 215 deg with respect to True North (see Fig. 1 for details of the LIST test site).

The data were recorded as ten-minute segments, each of which contains approximately 18,000 data points, at a sampling rate of 30 Hz (implying a Nyquist frequency of 15 Hz). Characterization of the inflow in this study relies on an array of five sonic anemometers mounted on three meteorological towers located approximately 30 m in front of the LIST turbine as shown in Fig. 1. The center tower is directly upwind of the LIST turbine. The other two towers are one rotor-disk radius to the left and right of the center tower. The five sonic anemometers are mounted as follows: at hub height which is 23 m from the ground; at the top and bottom of the rotor circle; and at positions left and right of the center of the rotor circle (see Fig. 2). Two additional meteorological towers located in front of the sister turbines, approximately 38 m away from the center tower on the left and right, were constructed to measure horizontal wind velocities at the hub height using cup anemometers. The additional inflow data from one of these two towers are used to study the coherence of the along-wind turbulence component at this greater lateral separation.

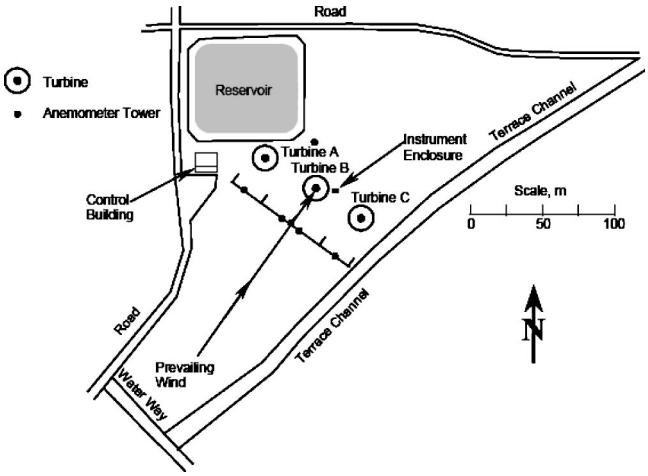

Fig. 1 Schematic view of the LIST test site showing the LIST turbine (Turbine B) and five meteorological towers

In preparation for the analysis, 291 of the available ten-minute data records were grouped into bins, depending on the horizontal mean wind velocity at hub height U_{hub} and the standard deviation of the same hub-height velocity, σ_{hub}. This was done in order to

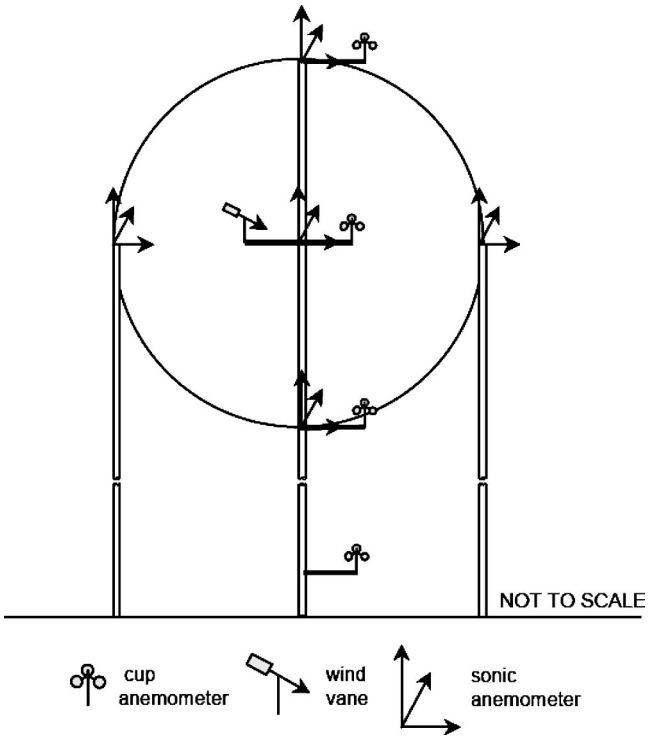

Fig. 2 Primary inflow instrumentation on the main meteorological towers upwind of the LIST turbine. Hub height is 23 m; anemometers on the center tower are spaced 8.5 m vertically apart; anemometers at hub height are spaced 7.7 m laterally apart.

Table 1 The number of ten-minute data sets in each bin characterized by the mean, U_{hub}, and standard deviation, σ_{hub}, of the hub-height horizontal wind velocity.

	U_{hub} (m/s)					
σ_{hub} (m/s)	7-9	9-11	11-13	13-15	15-17	>17
0.5-1.0	52	29	0	0	0	0
1.0-1.5	22	**33**	20	3	0	0
1.5-2.0	5	21	**25**	8	5	3
2.0-2.5	3	6	6	14	**14**	9
2.5-3.0	0	2	0	2	2	7

obtain a representative sample of data sets for each bin so that conclusions could be made about the dependence of coherence on these inflow parameters, regarded as primary by the wind energy community. The number of available data sets for each bin is shown in Table 1. We recognize that turbulence standard deviation does not affect coherence in a direct manner. A more appropriate inflow parameter for binning might have been the turbulence integral length scale L, as it is more directly related to the spatial coherence structure of wind fluctuations. However, we chose to bin the LIST data set in this study on the basis of mean wind speed and turbulence standard deviation because such binning is often used to define wind turbine classes for design purposes as specified in the IEC guidelines [5].

All the bins that contained a sufficient number of samples were analyzed; however, only results based on data sets from three bins are discussed in the following. These selected bins correspond to the boldfaced entries in Table 1. For simplicity, these are referred to as Bins A, B, and C in the following. The range in values of the mean U_{hub} and the standard deviation σ_{hub} of the horizontal wind speed at hub height for each of the three bins is shown in Table 2 along with the number of data sets available N_g. In passing, we mention that with binning on the basis of mean wind speed and turbulence length scale (instead of turbulence standard deviation) for the data sets studied here, a very similar numbers of data sets in three bins (like the Bins A, B, and C, here) is found. As a result, apart from the physically more sound reasons for choosing to bin on length scale when studying coherence, no improved statistical significance advantage is derived from such binning.

The LIST inflow data records collected by several anemometers as discussed above provide a good opportunity to study the coherence behavior of the three wind turbulence components for two different vertical separations of 8.5 and 17.0 m where the wind speed time series were measured by sonic anemometers located at three positions on the center tower mast. In addition, using the data collected by three sonic anemometers located at hub height on the three center towers as well as one cup anemometer on the far-right tower, the inflow coherence spectra for three lateral separations can be analyzed. However, since the mean wind direction during the measurement campaign was not perpendicular to the plane containing the wind speed sensor array, the actual lateral separations for coherence calculations are not equal to the horizontal distances between any two sensors and hence need to be corrected. This situation that results because the mean wind direction is not perpendicular to the plane of the mast array is illustrated graphically in Fig. 3. Correction to account for this effect is carried out by multiplying the actual horizontal distance between the two sensors under consideration by the cosine of the angle between a normal to the plane of the sensor array and the horizontal mean wind direction for each ten-minute data record. Then, these corrected lateral separations are averaged over all the ten-minute data sets in each bin. This finally leads to three different lateral separations for each bin that were used while reporting inflow coherence spectra results. These lateral separations are 6.5, 13.1, and 32.5 m for Bin A; 6.7, 13.4, and 33.2 m for Bin B; and 6.0, 12.1, and 29.9 m for Bin C as summarized in Table 3.

Table 2 Three bins selected for the numerical studies and the available number of ten-minute data sets, N_g.

Bin	U_{hub} (m/s)	σ_{hub} (m/s)	N_g
A	9-11	1.0-1.5	33
B	11-13	1.5-2.0	25
C	15-17	2.0-2.5	14

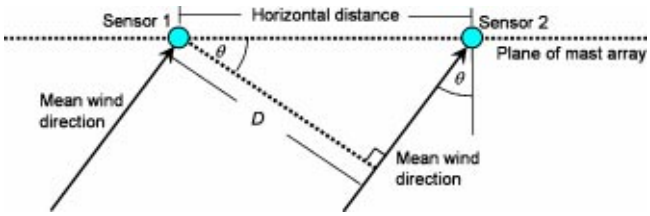

Fig. 3 Illustration of the corrected lateral separation D computed from the horizontal distance between two sensors and the angle between the mean wind direction and a normal to the plane of the mast array θ

III Coherence Estimation: A Review

A mathematical definition of the (magnitude-squared) coherence function, $\gamma^2(f)$, of two stationary random processes, p and q, may be given as

$$\gamma^2(f) = \frac{|S_{pq}(f)|^2}{S_{pp}(f)S_{qq}(f)} \tag{1}$$

where $S_{pp}(f)$ and $S_{qq}(f)$ are the one-sided (auto-)power spectral density functions of p and q, respectively, at frequency, f; and $S_{pq}(f)$ is the one-sided complex-valued cross-power spectral density function between the two processes. Note that some references refer to the coherence function as the root-coherence which is the absolute value of the normalized cross-power spectrum, i.e., $|\gamma(f)| = |S_{pq}(f)| / \sqrt{S_{pp}(f)S_{qq}(f)}$. Hereinafter, we will refer to the coherence function as the magnitude-squared coherence function [defined by Eq. (1)] and we will use either of these two terms (i.e., coherence or magnitude-squared coherence) interchangeably, unless specifically stated otherwise. It should be mentioned also that, for a homogeneous turbulence field, the quadrature spectrum (i.e., the imaginary part of the cross-power spectrum) will be relatively small when compared with the cospectrum (i.e., the real part of the cross-power spectrum). Hence, it is commonly assumed in wind turbulence simulation studies that the cross-spectral density function is real. As a result, the phase information conveyed by referring to a phase spectrum is generally considered less important than the magnitude-squared coherence or the root-coherence for wind turbine studies. Accordingly, here, the phase spectrum is excluded from our discussions. The coherence $\gamma^2(f)$, is always greater than or equal to zero and by Schwarz's inequal-

Table 3 Averaged angle between the mean wind direction and the plane of the mast array as well as the vertical and lateral separation distances available for estimating inflow coherence spectra for each bin.

		Separation distances (m.)				
		Lateral			Vertical	
Bin	Averaged angle (°)	Small	Intermediate	Large	Small	Intermediate
A	9.7	6.5	13.1	32.5	8.5	17.0
B	28.9	6.7	13.4	33.2		
C	−37.7	6.0	12.1	29.9		

ity, it always less than or equal to unity. For a finite-length data record, the coherence can be estimated from averaged estimates of the auto- and cross-spectra; namely,

$$\hat{\gamma}^2(f) = \frac{|\hat{S}_{pq}(f)|^2}{\hat{S}_{pp}(f)\hat{S}_{qq}(f)} \tag{2}$$

where the quantities with a caret indicate that each is estimated from the limited data (N_g data sets for each bin). Because of the use of limited data and of records of finite length, the estimates in Eq. (2) have unavoidable statistical errors. For example, an obvious distortion will occur if one tries to compute the coherence function by using only one realization of each of the two processes, p and q. For such an estimation procedure, the computed coherence function will be identically equal to unity at all frequencies. In practice, each sampled time series is therefore split into N subsegments to prevent this source of distortion. For N nonoverlapping realizations of a stationary, Gaussian random process, the bias (Bias) and the variance (Var) of the coherence spectrum estimate at any frequency due to time-record truncation effects were derived (Carter [11]) and may be expressed as

$$\text{Bias}(\hat{\gamma}^2) \approx \frac{1}{N} - \frac{2}{N+1}\gamma^2 + \frac{1!(N-1)}{\Pi_{i=1}^{2}(N+i)}\gamma^4 + \frac{2!(N-1)}{\Pi_{i=1}^{3}(N+i)}\gamma^6 \tag{3a}$$

$$\approx \frac{1}{N}(1-\gamma^2)^2 \quad \text{for large } N \tag{3b}$$

$$\text{Var}(\hat{\gamma}^2) \approx \frac{N-1}{N(N+1)}\left\{\frac{1}{N} + 2\gamma^2\frac{N-2}{N+2} - 2\gamma^4\frac{N(2N^2-N-2)+3}{\Pi_{i=1}^{3}(N+i)} + 2\gamma^6\frac{N(N^3-6N^2-N+10)-8}{\Pi_{i=1}^{4}(N+i)} + \gamma^8\frac{N(13N^4-15N^3-113N^2+27N+136)-120}{(N+2)\Pi_{i=1}^{5}(N+i)}\right\} \tag{4a}$$

$$\approx \begin{cases} \dfrac{1}{N^2} & \gamma^2 = 0 \\ \dfrac{2}{N}\gamma^2(1-\gamma^2)^2 & 0 < \gamma^2 \leqslant 1 \end{cases} \quad \text{for large } N \tag{4b}$$

Note that Eqs. (3*a*) and (4*a*) are approximate and result from truncating series expressions for the exact bias and variance of coherence estimates while Eqs. (3*b*) and (4*b*) involve further approximations that are applicable only when N is large. The reader is referred to the work of Carter [11] and Kristensen and Kirkegaard [12] for exact expressions for the bias and variance of coherence estimates. It is recognized that allowing for overlapping of subsegments can further reduce the statistical variability of the estimates because of the greater number of degrees of freedom used. Experimental investigation by Carter [11] where a Hanning data window was utilized suggests that 50% overlapping is an optimal choice as a compromise between reduction in standard error and computation time.

Besides conventional bias as predicted by Eq. (3*a*), bias power leakage effects may be introduced if the selected resolution bandwidth is wide relative to the actual range of frequencies associated with a peak in the spectrum. This category of bias, which is known as ''resolution bias'' may lead to large distortions near the peak of the spectrum. In studying turbulence components, this type of bias may be present due to the significant amount of energy at low frequencies. Even though a theoretical expression of this bias is not available, Jacobsen [13] concluded from numerical simulation studies that resolution bias effects will occur especially when the number of degree of freedom increases. This is typically associated with the number of (overlapping) subsegments used and when the coherence values are close to unity. Thus, under certain circumstances, this resolution bias may dominate the conventional bias [Eq. (3*a*)] resulting from a finite number of statistical realizations. Jacobsen [13] did not report any systematic variance dependency on power leakage from his experiments, indicating that the variance (or standard error) in coherence spectra may be estimated by Eq. (4*a*) alone.

Another source of bias in estimating coherence is due to possible time delay between the two signals p and q that can be easily detected either by simply observing the corresponding cross-covariance function of the two time series or by observing a linear trend in the phase spectrum. This source of bias might be important when studying coherence in turbulence components over large lateral separations.

IV Estimation Procedure

For each bin defined in Table 2, the wind velocities in the measured frame of reference are transformed into the standard micrometeorological coordinate system, defined as along-wind (u), across-wind (v), and vertical (w) components. Next, each ten-minute time series of interest is partitioned into a suitable number of 50% overlapped subsegments N_d, each of which is considered as a realization of the process for use in estimation of the spectra. Hence, each bin class yields a total of $N = N_d \times N_g$ realizations. Then, for each zero-mean realization (the mean is removed first), a detrending (assuming a linear trend), a prewhitening filter, and a Hanning data window multiplication are applied, before raw power and cross spectra are finally computed using the Fast Fourier Transform (FFT) algorithm. Next, these spectra derived from the realizations are averaged in each bin to obtain representative power spectral density functions and cross-power spectral density functions for use in Eq. (2) to compute the coherence spectrum, $\hat{\gamma}^2(f)$. This coherence estimate is then bias-corrected using Eq. (3*a*). Note that the prewhitening filter is applied here in order to reduce possible bias in power spectrum estimates in the low-frequency region due to leakage problems (Jenkins and Watts [14]; Schwartz and Shaw [15]). The prewhitening filter coefficients, based on a simple moving average model, were determined such that the power spectrum of the filtered turbulence signal is essentially ''white,'' resulting in less power at lower frequencies that ''leaks'' into the neighboring higher frequency region. By a trial-and-error procedure, the filter coefficients were found to be such that the prewhitened signal y_t, was equal to $1.01x_t - 1.00x_{t-1}$ where x is the original zero-mean, detrended signal. It is important to point out that detrending and prewhitening the inflow turbulence signal is essentially equivalent to applying linear high-pass filters to the signal, which will not affect coherence spectrum estimates. This is because the linear transfer functions will apply to both the auto- and cross-spectra and will eventually cancel out based on how they appear in the estimate of the coherence spectrum given by Eq. (2). Trend removal and prewhitening procedures, however, do directly influence auto- and cross-spectrum estimates individually. Disregarding either of these two procedures can lead to bias in auto- and cross-spectra individually, especially in the lowest frequency region (negligibly at higher frequencies). We accordingly employ these procedures here because even though they do not influence coherence estimates (our focus), we will briefly discuss auto-spectra estimates based on data and comparisons with theoretical model where such procedures help limit bias problems.

V Numerical Studies

Several issues related to coherence estimates based on the LIST field measurements are investigated. For simplicity, we will refer to power spectral density function of the along-wind (u), across-wind (v), and vertical (w) turbulence components as u-, v-, and w-power spectra, respectively. Similarly, for lateral and vertical separations studied, we refer to coherence functions of the along-

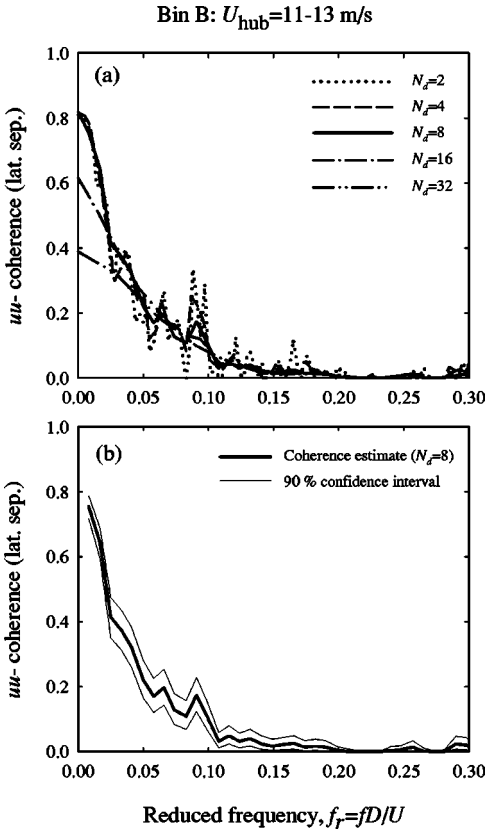

Fig. 4 (*a*) Estimates of *uu*-coherence spectra for a lateral separation distance of 13.4 m using data from Bin B and different numbers of subsegments N_d, (*b*) estimate of the *uu*-coherence spectrum and 90% confidence intervals using $N_d=8$

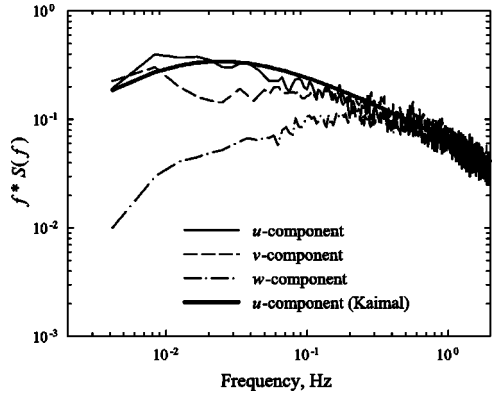

Fig. 5 Estimated power spectra of the along-wind (*u*), across-wind (*v*), and vertical (*w*) turbulence components for Bin B and comparison with the Kaimal along-wind turbulence spectrum [16] assuming a surface roughness of 0.5 cm.

wind, across-wind, and vertical turbulence components as *uu*-, *vv*-, and *ww*-coherences, respectively. Finally, we study cross-coherence between any two turbulence components at the center of the rotor circle and refer to these as *uv*-, *uw*-, and *vw*-coherences.

A Choices of Subsegment Length. To achieve good estimates of coherence spectra, it is necessary to use an appropriate number of overlapping subsegments that can provide satisfactorily small amounts of bias and standard error, without introducing much spectral distortion as discussed before. A large number of subsegments, which is associated with small individual subsegment length, might limit confidence intervals on the coherence estimate but it might introduce unacceptable spectral distortion and, thus, lose the fine structure of the coherence especially near the low frequency region where the coherence value is large. A rational approach was adopted in this study whereby bias-corrected (magnitude-squared) coherence spectra were estimated for different numbers of subsegments for a ten-minute time series. These estimates were then compared until an optimal number of subsegments was found. For the sake of illustration, we describe how this optimal number of subsegments was arrived at when estimating the *uu*-coherence for a lateral separation of 13.4 m using the 25 data sets that were taken from Bin B ($U_{\text{hub}}=11-13$ m/s and $\sigma_{\text{hub}}=1.5-2.0$ m/s). The same procedure may be applied for other turbulence components and/or for vertical separations. Figure 4(*a*) shows estimated *uu*-coherence spectra (for 13.4 m lateral separation) based on the use of 2, 4, 8, 16, and 32 subsegments in each ten-minute record. Figure 4(*b*) shows estimates of the coherence spectrum along with 90% confidence intervals with the optimal number of subsegments, equal to 8 here.

In this illustration, the number of subsegments N_d that is less than or equal to 8 does not cause severe distortion that can result from subsegments that are too short. A total of 200 realizations (8×25) is selected for estimating the coherence spectrum since this number provides the smallest standard error (compared to lower values of N_d that have similar bias) and still has very slight spectral distortion (compared to higher values of N_d that have systematically larger resolution bias). Using Eqs. (3*a*) and (4*a*), 90% confidence intervals were determined on the bias-corrected coherence spectra. These are shown in Fig. 4(*b*). Note that this conclusion on what is a suitable number of subsegments might be case-specific and the appropriate or optimal number of subsegments might vary from one case to another. Note also that the choice for the number of subsegments is not limited to integer powers of two. We selected these numbers as powers of 2 only for illustration purposes here.

In general, for the different separation distances that are used in this study, splitting the ten-minute time series into four to eight 50% overlapped segments will create individual realizations of about 2–4 m in length making it possible to resolve frequencies as low as 0.004–0.008 Hz with reasonable statistical confidence (and hence, avoid the problem of resolution expected at the low-frequency peak of coherence spectra). In passing, we point out that for 50% overlapping, each realization will have length equal to 10 minutes divided by $(N_d+1)/2$ and will be able to resolve frequencies as low as $(N_d+1)/1200$ Hz.

B Power Spectra. Power spectral density functions of the wind turbulence components were determined for the three Bins A, B, and C before using them to estimate coherence spectra. For the sake of brevity, in Fig. 5, we show power spectra only for Bin B for the three turbulence components at the center point of the rotor circle mast. The estimated spectra show that the energy in the along-wind turbulence component is slightly greater than that in the across-wind component in the low-frequency range and significantly greater than that in the vertical turbulence component. However, the power spectra for all three turbulence components asymptotically have the same slope and magnitude in the inertial subrange (high-frequency range). For the along-wind (u) turbulence component, the estimated power spectrum is compared with the Kaimal spectrum [16]. See the Appendix for a description of the Kaimal along-wind turbulence spectrum model used. A surface roughness length z_0 of 0.5 cm is used with the Kaimal model in the comparison (typical values of z_0 for mown grass terrain are about 0.1–1.0 cm). Comparison between the theoretical along-wind turbulence power spectrum and the estimated spectrum from

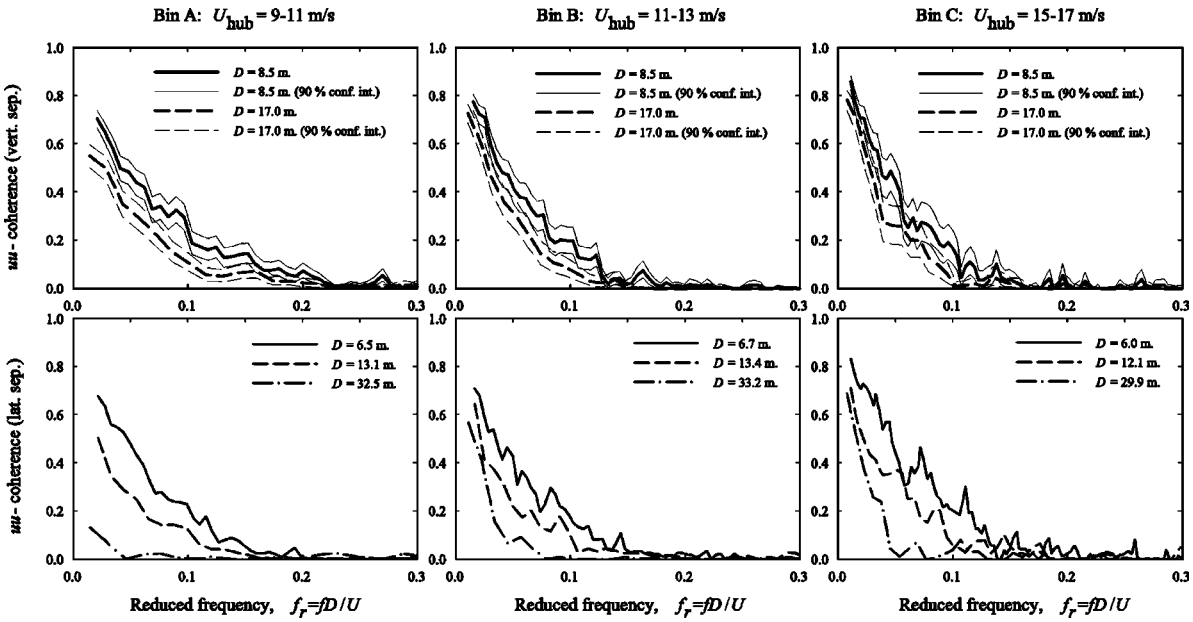

Fig. 6 Estimates of *uu*-coherence spectra for different vertical separations (top row); and for different lateral separations (bottom row) based on data from Bins A, B, and C

field data (at the height of 23 m) shows that the estimated spectrum agrees reasonably well over all frequencies with the Kaimal spectral model.

C Coherence Estimates, Empirical Models, and Influence of Separation. In this section, we study the inflow coherence of the along-wind turbulence component (uu-coherence) as estimated from the LIST field measurements and compare this measured coherence with predictions based on two commonly used empirical coherence models–the Davenport exponential model [17] and the IEC exponential model (Thresher et al. [18]; IEC/TC88 61400-1 [5]).

1 Davenport's Exponential Coherence Model. Based on numerous experimental results, Davenport [17] hypothesized that the coherence spectrum of the along-wind (u) turbulence component for different vertical separations could be described by an exponential function with a decay parameter, c, as follows:

$$\gamma^2(f) = \exp[-c(fD/U)] \tag{5}$$

where f represents the frequency of interest, D is the separation distance, and U is the mean wind speed at a specified reference or average height. As can be seen from Eq. (5), there are two key assumptions inherent in Davenport's empirical model. First, the coherence function is assumed to be dependent only on the rate of exponential decay, c, and on the reduced frequency, f_r (equal to fD/U). This implies no direct dependence of the uu-coherence spectrum on the vertical separation distance D as a separate variable; only an indirect dependence by virtue of the reduced frequency in Eq. (5). Second, the proposed coherence function in Eq. (5) approaches unity when the frequency approaches zero. Several researchers have extended this exponential format to model the coherence spectra for all three turbulence components and for both vertical and lateral separations where the applicable decay parameters in each case are estimated based on experimental results (see, for example, Jensen and Hjort-Hansen [19]). These models have been widely used and have been recommended in many references. For example, Simiu and Scanlan [20] recommend a decay parameter, c, of about 20 and 32 for the coherence spectra of the along-wind turbulence component for vertical and lateral separations, respectively. (Note that the values of 20 and 32 given here are twice as large as what are actually mentioned by Simiu and Scanlan [20] because their decay parameters there are for the root-coherence function, not the magnitude-squared coherence function, as we are discussing here.) Presently, we shall see that the coherence estimates from the LIST measurements are not in agreement with the Davenport model assumptions. It will be seen that the first assumption of the Davenport model may not be valid because the observed uu-coherence estimates are dependent on the separation distance as an additional independent parameter. Later, we shall see that the Davenport exponential model (which was originally proposed only for uu-coherence and vertical separations) may not be simply extended so as to be used for vv- and ww-coherence functions since the estimated coherence functions from measurements, especially for ww-coherence do not approach unity as the frequency approaches zero.

Coherence spectra are estimated based on the along-wind (u) turbulence time series available at several spatially distributed locations. Bins A, B, and C provided 33, 25, and 14 ten-minute samples, respectively, as seen in Tables 1 and 2. The various separation distances in the vertical and lateral directions available for each of the three bins are presented in Table 3.

For vertical separations of 8.5 and 17.0 m, the time series used to estimate the spectra were measured by sonic anemometers located at three positions on the center tower mast located approximately 30 m upwind of the LIST turbine: one at the top of the rotor circle, one at the center (i.e., at the hub height of 23 m), and one at the bottom of the rotor circle. The uu-coherence estimates (for the two vertical separations) along with their 90% confidence intervals are shown in Fig. 6 (top row) for the three different bins. It is observed that, for all bins, and especially for Bins A and B where there was a relatively large number of data sets available (and thus smaller statistical uncertainty), the uu-coherence even when plotted against the reduced frequency f_r (equal to fD/U) decreases as vertical separation increases from 8.5 to 17.0 m. This clearly shows a dependence of the uu-coherence on vertical separation distance. Nevertheless, if we determine the decay rate of the uu-coherence functions by fitting the Davenport model of Eq. (5) to the measured coherence over a range of reduced frequencies from 0 to 0.3, we find for Bin B, that the decay parameter c is approximately 17 and 25, respectively, for vertical separations of 8.5 and 17.0 m. For these separations, the estimated decay rates are in the same range as the decay parameter of 20 recommended

Table 4 Exponential decay rate, c, in the estimates uu-coherence spectra for different vertical and lateral separations based on fits to Davenport's expolnential coherence model.

	Davenport's Exponential Model Parameter (c)				
	Lateral Separations			Vertical Separations	
Bin	Small separation (6.0 to 6.7 m)	Intermediate separation (12.1 to 13.4 m)	Large separation (29.9 to 33.2 m)	Small separation (8.5 m)	Intermediate separation (17.0 m)
A	17	27	127	14	24
B	19	28	48	17	25
C	16	24	45	19	27

by Simiu and Scanlan [20]. Still, the decay parameter c increases with separation distance (from 17 to 25 here) and the decay rates recommended in standard references may clearly not be valid for larger separations. Note again that the dependence of the uu-coherence spectrum on the vertical separation distance observed from measurements in this study contradicts Davenport's exponential coherence model where this along-wind coherence function when expressed in terms of reduced frequency is assumed to be independent of separation.

For lateral separations (refer to Table 3 for the relevant separations for each bin studied), the ten-minute data sets used to estimate coherence spectra of the along-wind turbulence component were measured by three sonic anemometers located at the three main towers and a cup anemometer on the far right tower (see Fig. 1). All of these anemometers are at the hub height (23 m). Note again that the lateral separations used here for each bin have been corrected from the actual horizontal distances between the pertinent sensors to account for the direction of the mean wind during the measurement campaign which was not, in general, perpendicular to the mast array. The uu-coherence estimates for different lateral separations are shown in Fig. 6 (bottom row) for the three different bins. Again, when plotted against reduced frequency, f_r, the uu-coherence systematically decays faster with reduced frequency at larger lateral separations. Note that a recent study by Larsen and Hansen [8], where they estimated uu-coherence (for larger lateral separations than is the case here), suggested that there was no consistent dependence of coherence on spatial separation. Exponential decay rates (based on fitting the measured coherence spectra using Bin B data with the Davenport model) for separations of 6.7, 13.4, and 33.2 m are 19, 28, and 48, respectively, compared with about 32 in Simiu and Scanlan [20]. This again suggests a faster decay of uu-coherence with reduced frequency for increased lateral separations. A similar pattern is also found for Bins A and C as summarized in Table 4. Note that when comparing estimated decay rates for the uu-coherence spectra in Table 4 (at least for Bins A and B), it is found that over comparable separation distances in the lateral and vertical direction, this decay with reduced frequency is faster laterally than it is vertically. However, this difference is not significant in part due to uncertainty associated with coherence estimates based on a limited number of data sets. For the sake of comparison, it should be pointed out that Larsen and Hansen [8] also compared coherence decay at various lateral and vertical separations, and concluded that the decay is faster vertically (contrary to what we found here) but the lateral separations studied by them were much larger (79 and 170 m) than those considered here, and their vertical separations were not comparable to their lateral separations.

2 IEC Exponential Coherence Model. Our finding in the previous section is in agreement with the work by several other researchers (e.g. Kristensen and Jensen [21]; Mann et al. [6]) who showed, based on their experimental results, that Davenport's coherence assumptions may be invalid especially in situations where the spatial separation becomes large since this simple, empirical model fails to account for the reduction in coherence at low frequencies and large separations. To account for such limitations in the Davenport model, Thresher et al. [18] proposed another exponential coherence model that is also empirically based (as is the Davenport model). In this model, an additional term is present that involves the ratio of separation D to the coherence scale parameter L_c and that allows for reduction in coherence with increase in separation. This exponential model can be expressed as

$$\gamma^2(f) = \{\exp(-a[(fD/U)^2 + (bD/L_c)^2]^{1/2})\}^2 \tag{6}$$

This model is currently recommended in the IEC guidelines [5] for wind simulation and the decay parameters a and b are to be taken as 8.8 and 0.12, respectively, while the coherence scale parameter L_c is approximately 56 m for a wind turbine with a hub height of 23 m (see IEC/TC88 61400-1 [5] for details). In the present study, we will refer to this modified exponential model as the IEC exponential model. Similar to fits with the Davenport model, here we estimate the parameters a and b for the exponential model in Eq. (6) from estimates of the uu-coherence spectra. Again, fits of the estimated uu-coherences to the model were carried out for a range of reduced frequencies between 0 and 0.3. For illustration purposes, first we use data from Bin B alone. For vertical separations of 8.5 and 17.0 m, the estimated uu-coherence spectra were fit to the IEC exponential model and the decay parameter a was found to be 8.6 and 12.3, respectively, while the parameter b was about 0.00 and 0.02, respectively. Similarly, for lateral separations of 6.7 and 13.4 m, the decay parameter a was 9.4 and 13.6, respectively, while the parameter b was about 0.05 and 0.03, respectively. The fits based on these parameters are shown in Figs. 7(a) and 7(b) for the vertical and lateral separation cases, respectively.

It is observed that the IEC exponential model (with the associated parameters a and b) generally provides a good representation of the uu-coherence spectra for Bin B. Similar good fits of the exponential model for Bins A and C were also found. The estimated parameters for all three bins are summarized in Table 5. Note that these fits shown in Figs. 7(a) and 7(b) and the parameters summarized in Table 5 for the individual bins and separations were based on using a subset of the collected data for that bin and separation. Of greater interest is to employ all of the data and estimate the parameters a and b. Then, by using these estimated parameters, it would be interesting to see how the uu-coherence spectra at different separations compared with the exponential model using the overall estimated parameters a and b. For the vertical separations, over a range of reduced frequencies from 0.0 to 0.3, the overall least-squares fit parameters a and b for the exponential model for uu-coherence were 9.7 and 0.06, respectively, based on data recorded for two separations, 8.5 and 17.0 m. For lateral separations, these overall parameters were 9.7 and 0.13, respectively, based on data recorded over nine separations ranging from 6.0 m to 33.2 m. The overall parameters for both separation directions are included in Table 5. In the lateral separation case, these estimated parameters are fairly close to the values recommended in the IEC guidelines where a and b are 8.8 and 0.12, respectively. Fits based on the overall parameters ($a = 9.7$, $b = 0.13$) in the lateral separation case are shown in Fig. 8 for Bin B estimated coherence at three different separations. A

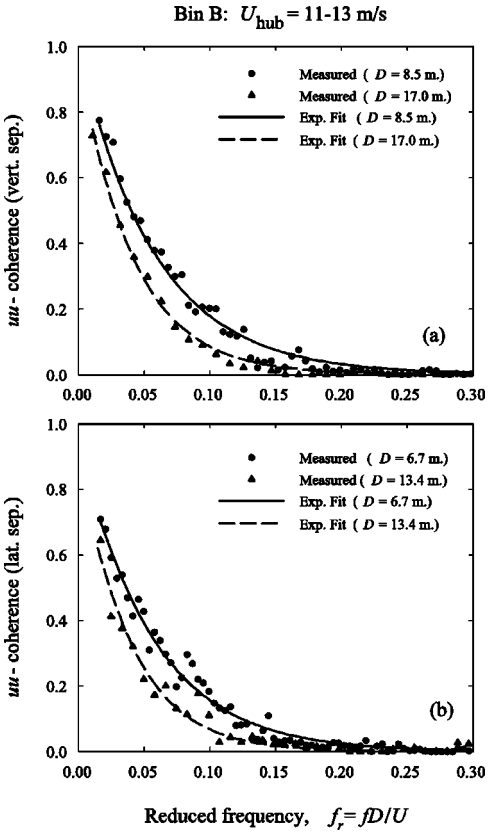

Fig. 7 Exponential fits based on the IEC exponential model in Eq. (6) for *uu*-coherence spectra with (*a*) vertical separations of 8.5 and 17.0 m and (*b*) lateral separations of 6.7 and 13.4 m using data from Bin B

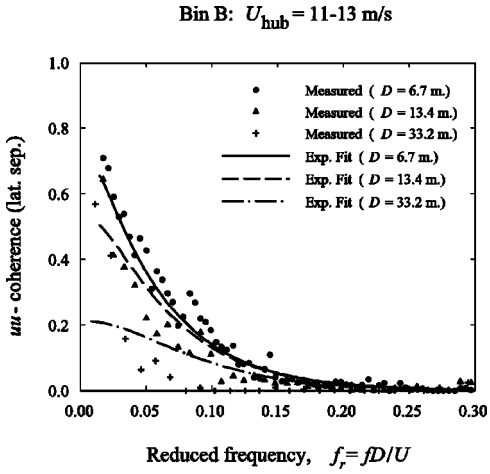

Fig. 8 Exponential fits based on the IEC exponential model in Eq. (6) for *uu*-coherence spectra with lateral separations of 6.7, 13.4, and 33.2 m using data from Bin B. The decay parameters used in this plot (a=9.7 and b=0.13) were estimated by fitting the model to all the measured *uu*-coherence spectra for all lateral separations and from all bins.

similar plot was not developed for the vertical separation case due to the limited number (two) of separations available for analysis. As one might expect, Fig. 8 shows that predictions of the exponential model are not as good as when the parameters a and b used were fit for each separation distance and bin individually. The IEC exponential model appears to work better at the smaller separations (6.7 and 13.4 m for Bin B). However, at the larger separation of 33.2 m, the model overpredicts coherence at reduced frequencies between 0.05 and 0.15 but significantly underpredicts coherence at lowest frequencies; the concave-down second curvature in the IEC exponential model in the low-frequency region appears to contradict what is observed in the uu-coherence estimated from data.

In summary, the Davenport exponential coherence model, though simple to use, may not be able to accurately describe the coherence structure in the wind turbulence components particularly for large separations because this model fails to account for reduction in coherence for low frequencies and large separations. The IEC exponential model is an improvement for uu-coherence since two parameters (instead of one in Davenport's model) are utilized to account for dependence on both reduced frequency and separation distance. Still, as shown in Fig. 8, the IEC coherence model predictions for uu-coherence at large lateral separations are quite different from coherence estimates based on field measurements especially at low frequencies. Because different coherence models employed in wind simulation procedures for wind turbine load calculations can sometimes lead to significant differences in design loads, more accurate theoretical coherence models may be required for better predictions of the coherence structure that will, in turn, lead to more realistic wind turbine design loads. Two such theoretical coherence models will be discussed later and compared with estimates based on the field data. Next, we compare the coherence structure in the different turbulent components as we examine uu-, vv- and ww-coherence spectra as estimated from the LIST field measurements.

D Coherence Structure of Each Turbulence Component In the previous section, we only discussed results related to coherence spectra of the along-wind (u) turbulence component–i.e., the uu-coherence. Coherence spectra for all three turbulence components (i.e., uu-, vv-, and ww-coherences) for two spatial separations are compared here. Figure 9 shows estimated coherence spectra of each turbulence component for small and intermediate lateral and vertical separations based on data in Bins A, B, and C.

Table 5 Paramters, *a* and *b*, of the IEC exponential model fits to the measured vertical and lateral coherence spectra.

	IEC Exponential Model Parameters (a,b) for Lateral Separations			IEC Exponential Model Paramters (a,b) for Vertical Separations	
Bin	Small separation (6.0 to 6.7 m)	Intermdiate separation (12.1 to 13.4 m)	Large separation (29.9 to 33.2 m)	Small separation (8.5 m)	Intermediate separation (17.0 m)
A	8.4, 0.06	12.2, 0.08	17.2, 0.17	7.0, 0.08	10.1, 0.08
B	9.4, 0.05	13.6, 0.03	21.2, 0.03	8.6, 0.00	12.3, 0.02
C	7.9, 0.02	11.4, 0.05	21.5, 0.03	9.4, 0.00	13.9, 0.01
All		**9.7, 0.13**			**9.7, 0.06**

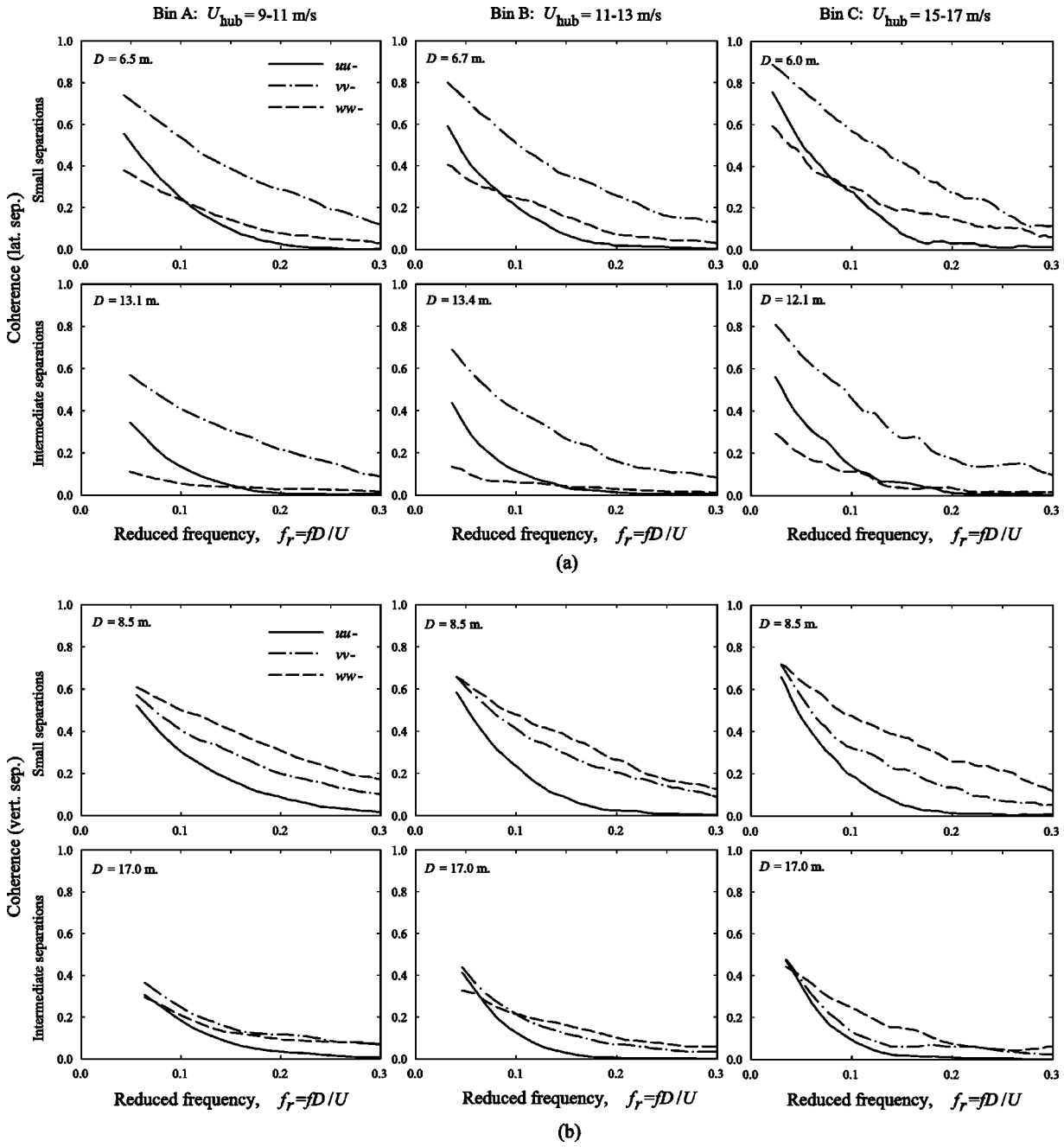

Fig. 9 Comparison of estimated coherence spectra for each turbulence component with (*a*) lateral separations (two upper rows) and (*b*) vertical separations (two lower rows) based on data from Bins A, B, and C.

For lateral separations, the wind velocity time series used for each component was measured by sonic anemometers mounted at hub-height level of the three center tower masts. It is seen in Fig. 9(a) that the across-wind (v) turbulence component is more coherent than the along-wind (u) and vertical (w) components for all bins. Comparing the uu- and ww-coherence, it is seen for all bins that the uu-coherence is larger than the ww-coherence in the low frequency range but lower at high frequencies. As expected, coherence in all three turbulence components decreases with increased lateral separation at all frequencies. At the larger lateral separations, it is seen that the vv-coherence is still the largest of the three components while the uu-coherence is higher than the ww-coherence over a larger-reduced frequency range. These plots in Fig. 9(a) show that the *relative* coherence levels for the three turbulence components agree with those based on the von Kármán coherence model [22] where isotropy was assumed in deriving the energy spectrum. When studying coherence spectra for different vertical separations [see Fig. 9(b)], the vertical turbulence component appears to be the most coherent followed by the across-wind and along-wind components. In the isotropic model, the vv- and ww-coherence depend on the direction of the separation. The vv-coherence for lateral separations is the same as the ww-coherence for vertical separations and vice versa. This might explain the change in relative importance of the vv- and ww-coherence among the three spectra shown in Figs. 9(a) and 9(b). Note, however, that the relative levels of the uu- and ww-coherence spectra for lateral separations are somewhat different from the relative levels of the uu- and vv-coherences for vertical separations. This observation is not in agreement with the isotropic model and thus suggests a lack of isotropy in the inflow

turbulence. To model the inflow coherence under these conditions more correctly, then, the isotropy constraint needs to be relaxed. Next, we study more closely the coherence structure of each turbulence component by comparing the estimated coherence spectra based on measurements with those predicted by two theoretical models–the isotropic von Kármán coherence model [22] and the Mann uniform shear coherence model [3] where local isotropy is not assumed.

E Comparing Coherence Structure of Each Turbulence Component With Theoretical Coherence Models. As has been already discussed, the Davenport coherence model fails to account for the decrease in coherence at low frequencies and for large separations while the IEC exponential coherence model predictions for large separations do not adequately match coherence estimates from field measurements. Hence, alternative theoretical coherence models might be considered instead of empirical models for use in predicting inflow coherence. Here, we consider two such theoretical coherence models that are available in the literature. These include (i) the isotropic von Kármán turbulence model [22] where isotropy is assumed in deriving the energy spectrum and (ii) the Mann uniform shear turbulence model [3] where the isotropic von Kármán energy spectrum is assumed to be rapidly distorted by a uniform, mean velocity shear. Predictions based on these theoretical models will be compared with the measured coherence spectra for all turbulence components and for various lateral spatial separations. For the sake of comparison with an empirical model, the IEC exponential model discussed previously will also be included whenever the uu-coherence spectra are studied. (There is no corresponding IEC exponential coherence model available for vv- and ww-coherence spectra in the IEC standard.) The isotropic von Kármán coherence model and the IEC exponential model can be conveniently described using available closed-form mathematical functions. Both these models are currently included into the IEC standard [5] and are recommended for use in wind turbine load calculations. The Mann uniform shear model, on the other hand, requires greater computational effort since the influence of shear or vertical mean speed gradient (assumed uniform) from the surface on isotropic turbulence is included in the model. Because of its complex formulation, the Mann coherence spectrum offers no simple analytical solution but rather requires numerical integration involving the sheared three-dimensional velocity spectral tensor, Φ_{ij} (where i and j are equal to 1, 2, and 3 for the along-wind, across-wind, and vertical turbulence components, respectively). Expressions for the magnitude-squared coherence spectra based on the von Kármán and the Mann models are provided in the Appendix while that for the IEC exponential model was shown previously in Eq. (6).

Notice that one requires the parameters a and b and the coherence scale parameter L_c in order to obtain the IEC exponential coherence spectra. For the von Kármán model, information on the isotropic integral length scale L is necessary while the Mann coherence model requires an isotropic scale parameter l (which is proportional to the isotropic integral scale L), and one additional nondimensional shear distortion parameter s to quantify the influence of the shear due to the ground surface. Obviously, all of these parameters are site-dependent and their values can be estimated only from field measurements at the site under consideration. In most situations, however, this site-dependent information is not readily available and, in such cases, these various parameters can only be approximated. Since it is our intention to assess the va-

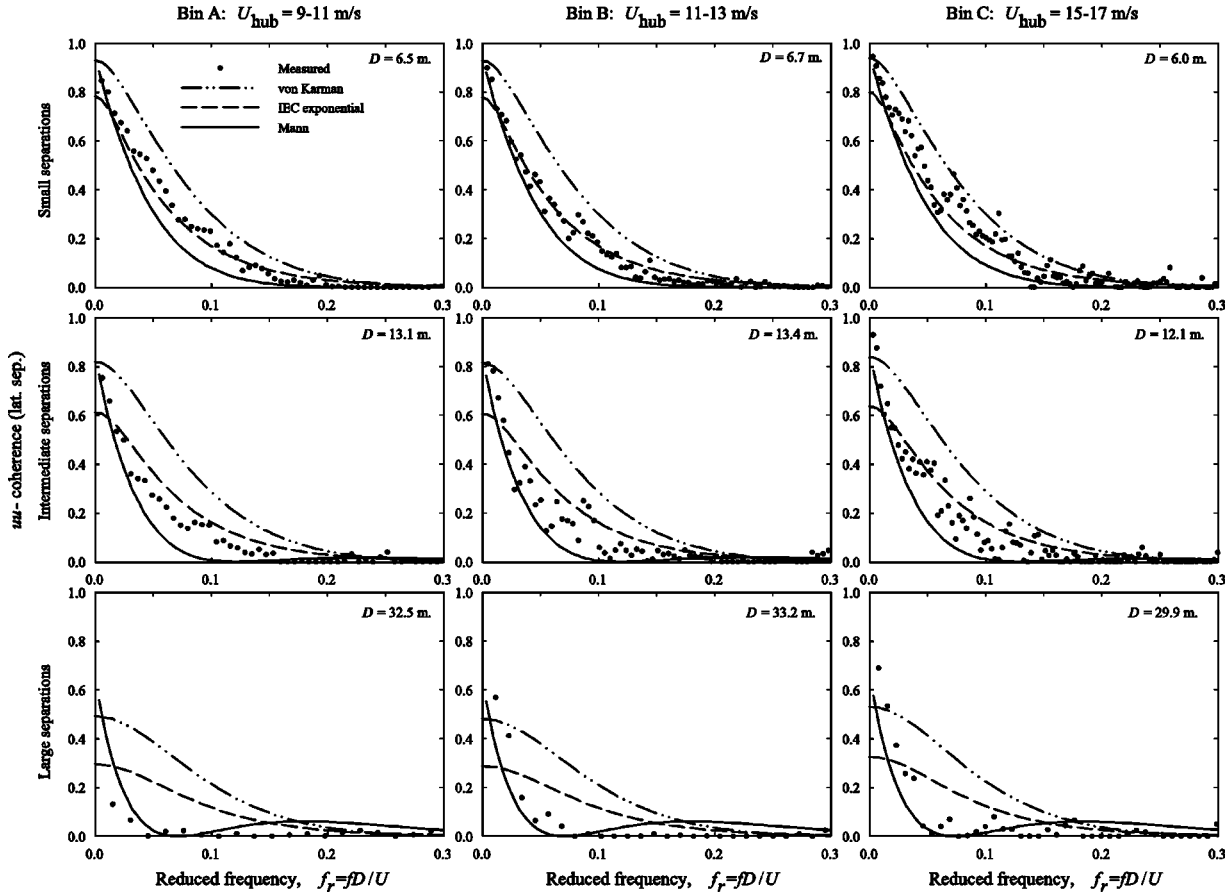

Fig. 10 Comparison of the estimated uu-coherence spectra for lateral separations (based on data sets from three bins) with the IEC modified exponential (a=8.8, b=0.12, L_c=56 m), the von Kármán (L=56 m), and the Mann (s=3.9, l=14 m) models

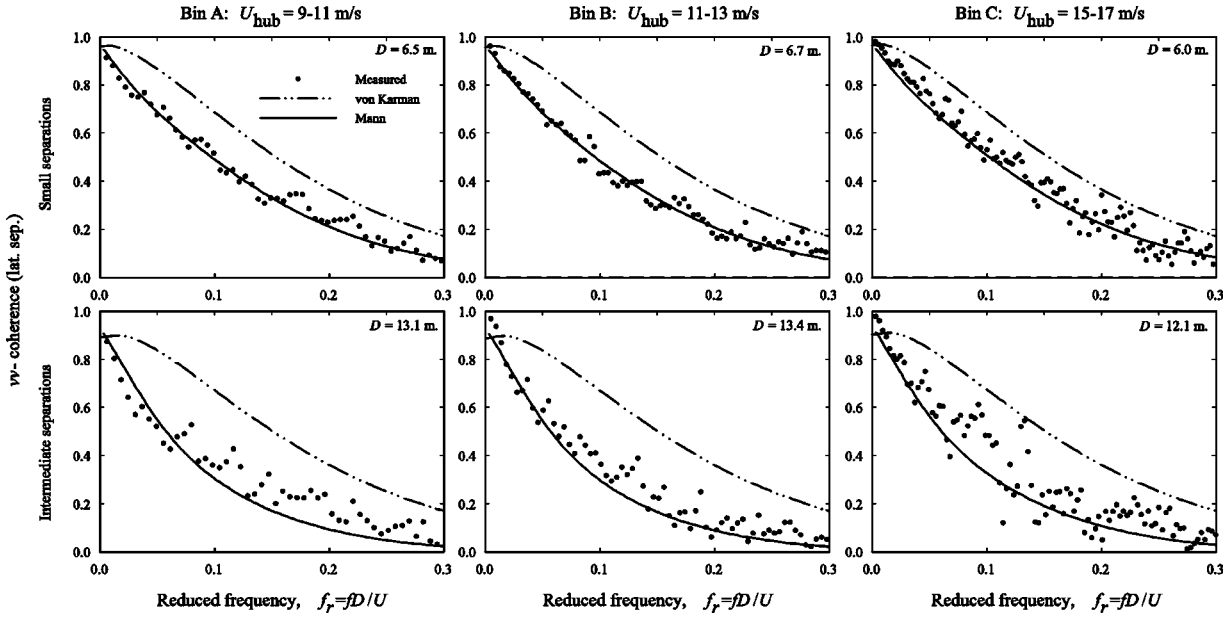

Fig. 11 Comparison of the estimated *vv*-coherence spectra for lateral separations (based on data sets from three bins) with the von Kármán (L=56 m) and the Mann (s=3.9, l=14 m) models

lidity of the existing coherence models recommended in the wind turbine design code, all the parameters used here are taken directly from the code; they are not estimated from the field measurements. For example, numerical values for the required parameters a, b, L_c, and L are each taken from the IEC standard [5]. As was mentioned before, the recommended decay parameters a and b in the IEC guidelines are 8.8 and 0.12, respectively, and for this particular case where the hub height is 23 m, the suggested value for both L and L_c is approximately 56 m (see IEC/TC88 61400-1 [5] for details). For the Mann model, the two parameters l and s may be approximately obtained by performing a least-squares fit of the model's coherence spectra to the Kaimal model [16] instead of to estimated coherence spectra based on measurements. Mann [23] carried out such least-squares fits from which s was found to be 3.9 while l is 0.59 times the height of interest (hence, l is taken to 14 m here). Note that estimating these parameters from field measurements might provide a closer match to measured coherence spectra but this is not done here.

Figure 10 shows estimated uu-coherence spectra from measurements for Bins A, B, and C at three different lateral separations together with spectra predicted by the three models. When considering small lateral separations, it is seen from the top row in Fig. 10 that all three models predict similar levels of coherence. However, the IEC exponential model appears to provide the best prediction of the three models for uu-coherence, except in the very low frequency range where the Mann model provides the better prediction. The estimated uu-coherence from data is typically lower than that from the von Kármán turbulence model for

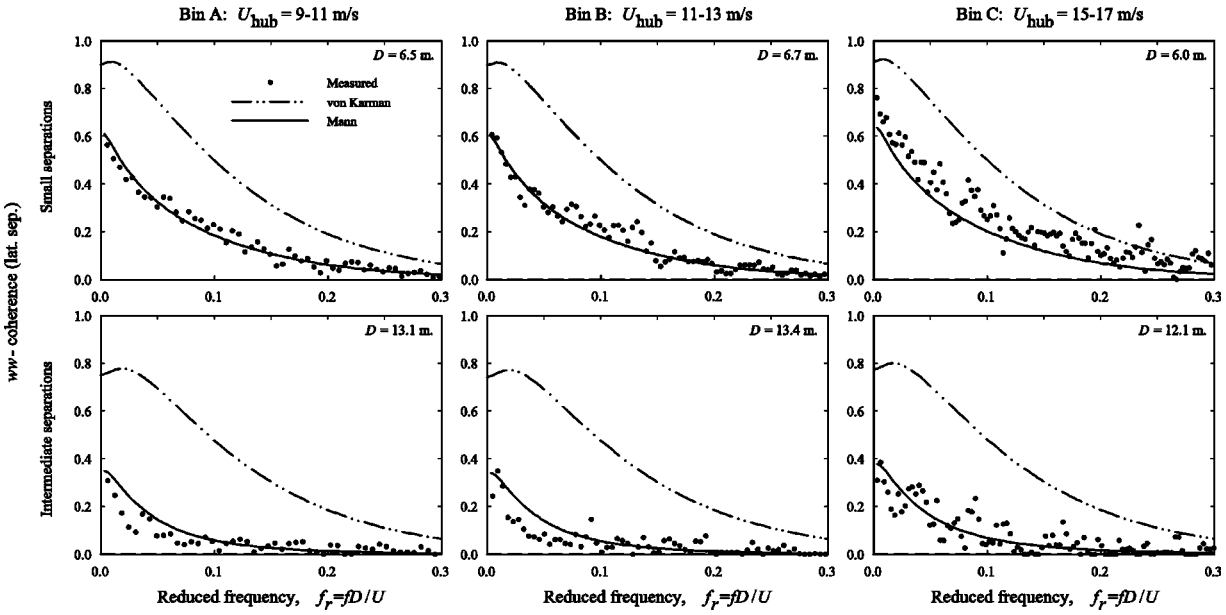

Fig. 12 Comparison of the estimated *ww*-coherence spectra for lateral separations (based on data sets from three bins) with the von Kármán (L=56 m) and the Mann (s=3.9, l=14 m) models

all three bins. For larger lateral separations (as shown in the two lower rows of Fig. 10), the three models predict very different coherence behavior from each other. The von Kármán and the IEC exponential models appear to predict similar trends (though the von Kármán model predictions are always higher) where the spectra at low frequency region lose their exponential character and, as a result, do no approach unity at these low frequencies. The Mann model, on the other hand, predicts much higher coherence gradients (faster decays) in the low-frequency range. It is evident from the figures that especially for the larger spatial separations, the Mann coherence model is able to capture higher coherence levels and faster decays (with reduced frequency) in uu-coherence spectrum in the low-frequency region, consistent with field measurements for the higher wind speed bins (B and C). The coherence behavior predicted by the other two models is grossly different from what was observed in the field measurements.

Figures 11 and 12, respectively, show estimated vv- and ww-coherence spectra from measurements for Bins A, B, and C at small and intermediate lateral separations compared with predictions based on the von Kármán and Mann models. It is clear from Fig. 12 that the ww-coherence spectra estimated from data do not approach unity at very low frequencies. In fact, at the intermediate separations of around 12–13 m, these ww-coherence function values fall below 0.3 at low frequencies. This is an obvious contradiction with one of the Davenport model assumptions mentioned earlier. This, in turn, suggests that extending the original Davenport coherence model of Eq. (5) (initially proposed for uu-coherence with vertical separations) to use for other turbulence components, especially for the vertical turbulence (w) component is clearly not suitable. When comparing the estimated vv- and ww-coherence spectra from data with von Kármán and Mann model predictions, it is observed that the Mann coherence model predicts smaller coherence values compared with the von Kármán model for both turbulence components. More importantly, the estimated coherence spectra based on the LIST data sets appear to agree very well with the Mann model predictions over all separations and for all three bins studied.

F Cross-coherence. Cross-coherence spectra based on two distinct turbulence components (uv-, uw-, and vw-) recorded at the same point in space (here, the center of the rotor circle with a height of 23 m) were estimated and the results are summarized in Fig. 13. The figure shows no significant correlation between the along-wind (u) and the across-wind (v) turbulence components nor between the across-wind (v) and vertical (w) turbulence components in any of the three bins. This finding is consistent with the isotropic von Kármán model. It is also consistent with the Mann uniform shear coherence model where the uv- and vw-coherence spectra are theoretically zero at all frequencies, due to the antisymmetric character of the velocity spectral tensor components Φ_{12} and Φ_{23} in these two models. This is different for the correlation between the along-wind and vertical components where larger estimates of cross-coherence were observed. This observation is contradictory to the von Kármán coherence model where the derived uw-coherence is expected to be zero at all frequencies. Note that the uw-coherence is related to the square of the friction velocity and, thus, to the influence of wind shear. The von Kármán model assumes isotropy and does not take the wind shear effect into account; this, in turn, leads to failure to correctly predict the uw-coherence estimated from the field data. On the other hand, the Mann model has a spectral tensor component Φ_{13}, which is symmetric with respect to the wave number of the across-wind turbulence component; thus, providing a nonzero uw-coherence spectrum as can be seen in Fig. 13. It is clear, though, that the Mann model appears to overestimate the uw-coherence function for all the three bins studied. This finding is in agreement with the work by Mann [3] where he reported that the model overestimates uw-coherence, and suggested that a more complex model where the inhomogeneous rapid distortion theory (Lee and Hunt [24]) is included might provide better predictions for this cross-coherence. The present study suggests that it might be important to model uw-coherence (e.g., by using the Mann model) when simulating inflow to derive design loads for wind turbines, especially if additional studies can confirm that incorporating this cross-coherence could lead to significant changes in turbine design loads.

G A Note on Atmospheric Stability. It is important to mention that the coherence spectrum for turbulence components of the inflow depends to some degree on atmospheric stability conditions. Theoretical models (such as the isotropic von Kármán and the Mann uniform shear coherence models) available in the literature are usually derived based upon the assumption that neutral or stable atmospheric conditions exist. Since there were a limited number of data sets available for this particular study, we did not discard any of the measured wind speed time series, some of which might have been associated with unstable conditions. The resulting mixture of data sets of different stability conditions may account for some of the differences found between coherence spectra predicted by empirical/theoretical models and estimates based on the measured data as discussed in this paper.

VI Conclusions

In this study, we examined spatial statistics using the LIST program's measured inflow turbulence by obtaining estimates of power and coherence spectra using ten-minute segments of three components of the wind velocity at several different locations. Coherence spectra for different lateral and vertical separations were studied as were cross-coherence spectra between distinct turbulent components. Estimation errors associated with coherence spectra described by bias, variance, and confidence intervals were also dis-

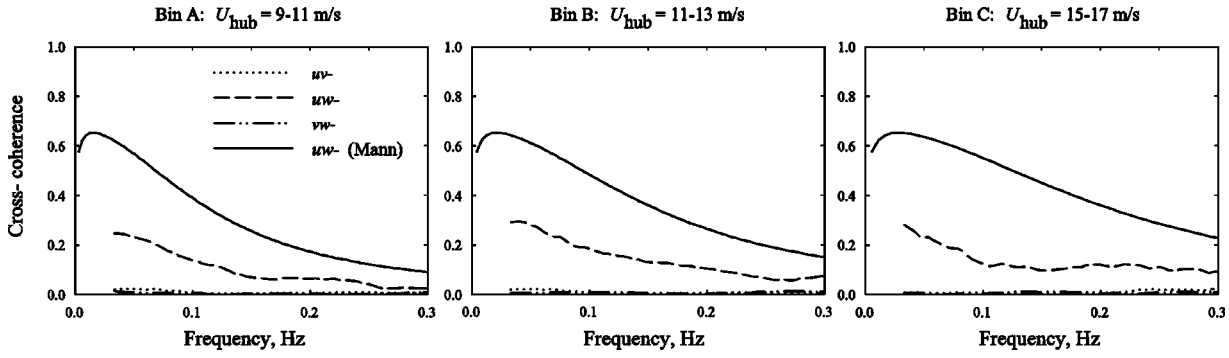

Fig. 13 Estimates of cross-coherence spectra at the center of the rotor circle for the turbulence components taken two at a time based on data from Bins A, B, and C, compared with the Mann uniform shear model. (The isotropic von Kármán model predicts zero cross-coherences at all frequencies.)

cussed. Results obtained for the three different bins of data defined in Table 2 allow us to make the following general conclusions:

- The along-wind coherence spectra for both vertical and lateral separations, when expressed in terms of reduced frequency, decays faster with increasing separation.
- The Davenport model exponential decay parameter was found to depend on the separation distance. The assumption that the inflow coherence spectrum approaches unity at zero frequency is inconsistent with observed coherence spectra for the across-wind and vertical turbulence components. Hence, extending the Davenport coherence model hypotheses for use with these turbulence components is not appropriate.
- The IEC modified exponential model predictions of the along-wind coherence for small lateral and vertical separations matched the estimated coherence from data fairly well, except at very low frequencies. There, this model predicts lower coherence than was estimated from data. At large separations and low frequencies, the IEC modified exponential model fails to describe the observed fast decay of coherence with reduced frequency.
- The *relative* coherence levels of the along-wind, across-wind, and vertical turbulence components for the different lateral separations as estimated based on data were in accordance with the von Kármán model. The different relative levels of coherence found when considering vertical separations may indicate a lack of isotropy in the turbulence structure.
- Using a required model parameter value as recommended by the IEC standard, the von Kármán model generally overestimated coherence when compared to estimates from data. This was found especially so when studying the coherences of the across-wind and vertical turbulence components, but was also seen when studying the coherence of the along-wind turbulence component, and especially at large lateral separations.
- Overall, the Mann uniform shear coherence model based on parameters fit with the Kaimal turbulence spectra appears to agree reasonably well with the estimated coherence spectra from data for all three turbulence components although it did underestimate the along-wind coherence for small lateral separations. In particular, the Mann model predicts low-frequency coherence better than other models studied, and the model does especially well compared to the von Kármán model for across-wind and vertical coherence predictions.
- Estimated cross-coherence between the along-wind and across-wind turbulence components as well as between the across-wind and vertical components is far less significant than that between the along-wind and vertical turbulence components. This cross-coherence cannot be predicted by the isotropic von Kármán model since the influence of the shear is not included in the model, while the Mann model generally overpredicted the cross-coherence between the along-wind and vertical turbulence components.

Acknowledgments

The authors gratefully acknowledge the financial support provided by Grant No. 003658-0272-2001 awarded through the Advanced Research Program of the Texas Higher Education Coordinating Board. They also acknowledge additional support from Sandia National Laboratories by way of Grant No. 30914. The authors are grateful to Sandia's Dr. Herbert J. Sutherland for providing us with the field data from the LIST program and they thank him and Dr. William E. Holley for their helpful insights and suggestions. Finally, the authors are pleased to acknowledge three anonymous reviewers who helped us with very useful comments and discussions related to this paper.

Appendix

A Kaimal Spectrum Model for Longitudinal Wind Velocity Turbulence (Kaimal et al. [16]).

$$S_u(f) = \frac{105 u_*^2 (z/U)}{[1+33(fz/U)]^{5/3}}$$

where z is the height above the ground in meters, u_* is the shear velocity, $u_* \approx 0.4U/\ln(z/z_0)$, and z_0 is the surface roughness in meters.

B The Isotropic von Kármán Coherence Model for Lateral Separations (von Kármán [22]).

$$\gamma^2(f) = \left\{ \frac{2^{1/6}}{\Gamma(5/6)} \left[\zeta^{5/6} K_{5/6}(\zeta) - \frac{1}{2} \zeta^{11/6} K_{1/6}(\zeta) \right] \right\}^2$$

for along-wind turbulence component,

$$\gamma^2(f) = \left\{ \frac{2^{1/6}}{\Gamma(5/6)} \left[\zeta^{5/6} K_{5/6}(\zeta) + \frac{3(2\pi fD/U)^2}{3\zeta^2 + 5(2\pi fD/U)^2} \zeta^{11/6} K_{1/6}(\zeta) \right] \right\}^2$$

for across-wind turbulence component,

$$\gamma^2(f) = \left\{ \frac{2^{1/6}}{\Gamma(5/6)} \left[\zeta^{5/6} K_{5/6}(\zeta) - \frac{3(D/aL)^2}{3\zeta^2 + 5(2\pi fD/U)^2} \zeta^{11/6} K_{1/6}(\zeta) \right] \right\}^2$$

for vertical turbulence component,

where $\zeta = 2\pi\sqrt{(fD/U)^2 + (0.12D/L)^2}$, $a = \dfrac{\Gamma(1/3)}{\sqrt{\pi}\,\Gamma(5/6)}$,

L is the isotropic turbulence integral scale, $L = 3.5\Lambda$, Λ is the turbulence scale parameter (IEC/TC88 61400-1 [5]), $\Gamma(\,)$ is the Gamma function, and $K_\nu(\,)$ is the modified Bessel function of order ν.

Note that in the isotropic model, the vv- and ww-coherence functions depend on the separation direction while the uu-coherence function does not. The vv-coherence for vertical separations is the same as the ww-coherence for lateral separations and vice versa.

C The Mann Uniform Shear Model (Mann [3]). The Mann spectral tensor components $\Phi_{ij}(k_1, k_2, k_3)$ are given by

$$\Phi_{11}(k_1,k_2,k_3) = \frac{E(k_0)}{4\pi k_0^4}[k_0^2 - k_1^2 - 2k_1(k_3 + \beta(k)k_1)\zeta_1 + (k_1^2 + k_2^2)\zeta_1^2],$$

$$\Phi_{22}(k_1,k_2,k_3) = \frac{E(k_0)}{4\pi k_0^4}\{k_0^2 - k_2^2 - 2k_2[k_3 + \beta(k)k_1]\zeta_2 + (k_1^2 + k_2^2)\zeta_2^2\},$$

$$\Phi_{33}(k_1,k_2,k_3) = \frac{E(k_0)}{4\pi k^4}(k_1^2 + k_2^2),$$

$$\Phi_{12}(k_1,k_2,k_3)=\frac{E(k_0)}{4\pi k_0^4}\{-k_1k_2-k_1[k_3+\beta(k)k_1]\zeta_2 - k_2[k_3+\beta(k)k_1]\zeta_1+(k_1^2+k_2^2)\zeta_1\zeta_2\}$$

$$\Phi_{13}(k_1,k_2,k_3)=\frac{E(k_0)}{4\pi k_0^2k^2}\{-k_1[k_3+\beta(k)k_1]+(k_1^2+k_2^2)\zeta_1\}$$

$$\Phi_{23}(k_1,k_2,k_3)=\frac{E(k_0)}{4\pi k_0^2k^2}[-k_2[k_3+\beta(k)k_1]+(k_1^2+k_2^2)\zeta_2],$$

and the Mann coherence spectrum for spatial separations normal to the along-wind direction is given by

$$\gamma_{ij}^2(f)=\frac{\left|\int_{-\infty}^{+\infty}\int_{-\infty}^{+\infty}\Phi_{ij}(k_1,k_2,k_3)e^{-\iota k_2\delta_2}e^{-\iota k_3\delta_3}dk_2dk_3\right|^2}{\int_{-\infty}^{+\infty}\int_{-\infty}^{+\infty}\Phi_{ii}(k_1,k_2,k_3)dk_2dk_3\int_{-\infty}^{+\infty}\int_{-\infty}^{+\infty}\Phi_{jj}(k_1,k_2,k_3)dk_2dk_3}$$

where i and $j=1$, 2, 3 for the along-wind, across-wind, and vertical turbulence components, respectively, δ_1, δ_2, δ_3 are the nondimensional spatial separation vector components, defined as $\delta_i=D_i/l$, k_1,k_2,k_3 are the nondimensional spatial wave numbers, defined as $k_i=2\pi fl/U$, l is an isotropic scale parameter proportional to the isotropic integral length scale L,

$$k=\sqrt{k_1^2+k_2^2+k_3^2},$$

$$k_0=\sqrt{k^2+2\beta(k)k_1k_3+[\beta(k)k_1]^2},$$

$$\zeta_1=C_1-(k_2/k_1)C_2,$$

$$\zeta_2=(k_2/k_1)C_1+C_2,$$

$$C_1=\frac{\beta(k)k_1^2\{k_1^2+k_2^2-k_3[k_3+\beta(k)k_1]\}}{k^2(k_1^2+k_2^2)},$$

$$C_2=\frac{k_2k_0^2}{(k_1^2+k_2^2)^{3/2}}\arctan\left(\frac{\beta(k)k_1\sqrt{k_1^2+k_2^2}}{k_0^2-[k_3+\beta(k)k_1]\beta(k)k_1}\right),$$

$E(k)=\dfrac{1.453k^4}{(1+k^2)^{17/6}}$, the nondimensional, von Kármán isotropic energy spectrum,

$$\beta(k)=\frac{s}{k^{2/3}\sqrt{{}_1F_2\left(\frac{1}{3},\frac{17}{6},\frac{4}{3},-k^{-2}\right)}},$$

and s is the shear parameter, while ${}_1F_2(\ )$ is the hypergeometric function.

References

[1] Nelson, L. D., Manuel, L., Sutherland, H. J., and Veers, P. S., 2003, "Statistical Analysis of Inflow and Structural Response Data from the LIST Program," *Proceedings of the ASME Wind Energy Symposium*, paper No. AIAA-2003-0867, Reno, NV, pp. 276-282.

[2] Veldkamp, D., 2003, "Influence of Wind Field Generation Methods on Wind Turbine Fatigue Loads," *European Wind Energy Conference and Exhibition*, Madrid, Spain.

[3] Mann, J., 1994, "The Spatial Structure of Neutral Atmospheric Surface-Layer Turbulence," J. Fluid Mech., **273**, pp. 141–168.

[4] Veers, P. S., 1988 "Three-dimensional Wind Simulation," Report No. SAND 88-0512, Sandia National Laboratory, Albuquerque, NM.

[5] IEC/TC88 61400-1, 1998, "Wind Turbine Generator Systems Part 1: Safety Requirements," International Electrotechnical Commission (IEC), 2nd ed., Geneva, Switzerland.

[6] Mann, J., Kristensen, L., and Courtney, M. S., 1991, "The Great Belt Coherence Experiment," Report No. R-596, Risø National Laboratory, Roskilde, Denmark.

[7] Schlez, W., and Infield, D., 1998, "Horizontal, Two Point Coherence for Separations Greater than the Measurement Height," Boundary-Layer Meteorol., **87**, pp. 459–480.

[8] Larsen, G. C., and Hansen, K. S., 2003, "Spatial Coherence of the Longitudinal Turbulence Component," *European Wind Energy Conference and Exhibition*, Madrid, Spain.

[9] Sutherland, H. J., Jones, P. L., and Neal, B., 2001, "The Long-Term Inflow and Structural Test Program," *Proceedings of the ASME Wind Energy Symposium*, paper No. AIAA-2001-0039, pp. 1-12, Reno, NV, pp. 162-172.

[10] Jones, P. L., Sutherland, H. J., and Neal, B. A., 2001, "LIST/BMI Turbines Instrumentation and Infrastructure," Report No. SAND2001-1642, Sandia National Laboratories, Albuquerque, NM.

[11] Carter, G. C., 1972, "Estimation of the Magnitude-Squared Coherence Function," Report No. 4343, Naval Undersea Systems Center, New London Laboratory, CT.

[12] Kristensen, L., and Kirkegaard, P., 1986, "Sampling Problems with Spectral Coherence," Report No. R-526, Risø National Laboratory, Roskilde, Denmark.

[13] Jacobsen, S., 1993, "Statistics of Leakage-Influenced Squared Coherence Estimated by Bartlett's and Welch's Procedures," IEEE Trans. Signal Process., **41**, No. 1, pp. 267–277.

[14] Jenkins, G. M., and Watts, D. G., 1968, *Spectral Analysis and its Applications*, Holden-Day Inc., San Francisco, CA.

[15] Schwartz, M., and Shaw, L., 1975, *Signal Processing: Discrete Spectral Analysis, Detection, and Estimation*, McGraw-Hill, New York.

[16] Kaimal, J. C., Wyngaard, J. C., Izumi, Y., and Cote, R. O, 1972, "Spectral Characteristics of Surface Layer Turbulence," Q. J. R. Meteorol. Soc., **98**, pp. 563–598.

[17] Davenport, A. G., 1961, "The Spectrum of Horizontal Gustiness near the Ground in High Winds," Q. J. R. Meteorol. Soc., **87**, pp. 194–211.

[18] Thresher, R. W., Holley, W. E., Smith, C. E., Jafarey, N., and Lin, S.-R., 1981, "Modeling the Response of Wind Turbines to Atmospheric Turbulence," Report No. RL0/2227-81/2, Department of Mechanical Engineering, Oregon State University, OR.

[19] Jensen, N. O., and Hjort-Hansen, E., 1977, "Dynamic Excitation of Structures by Wind–Turbulence and Response Measurements at the Sotra Bridge," Report No. STF71 A78003, Trondheim-NTH, Norway.

[20] Simiu, E., and Scanlan, R. H., 1996, *Wind Effects on Structures: Fundamentals and Applications to Design*, 3rd Ed., Wiley, New York.

[21] Kristensen, L., and Jensen, N. O., 1979, "Lateral Coherence in Isotropic Turbulence and in the Natural Wind," Boundary-Layer Meteorol., **17**, pp. 353–373.

[22] von Kármán, T., 1948, "Progress in the Statistical Theory of Turbulence," Proc. Natl. Acad. Sci. U.S.A., **34**, pp. 530–539.

[23] Mann, J., 1998, "Wind Field Simulation," Probab. Eng. Mech., **13**, pp. 269–282.

[24] Lee, M. J., and Hunt, J. C. R., 1989, "The Structure of Sheared Turbulence near a Plane Boundary," 7th Symposium on Turbulent Shear Flows, Stanford University, CA.